Check for updates

Received: 21 January 2020 | Revised: 6 July 2020 | Accepted: 26 July 2020

DOI: 10.1111/jace.17400

ORIGINAL ARTICLE

Journal of the American Ceramic Society

Empirical models of trigonal distortions and polarization in perovskites

Evan Smith[1] | **Olivia Wander**[2] | **Rick Ubic**[1]

[1]Micron School of Materials Science & Engineering, Boise State University, Boise, ID, USA

[2]Department of Materials Science & Engineering, North Carolina State University, Raleigh, NC, USA

Correspondence
Rick Ubic, Micron School of Materials Science & Engineering, Boise State University, 1910 University Drive, Boise, Idaho, 83725, USA.
Email: rickubic@boisestate.edu

Abstract

Correlative models derived from empirical relations describing synthesis-structure relationships are essential to guiding and improving future research and development of functional materials, yet few models exist for the prediction of structural distortions in perovskites. In this work, a data-mining approach has been employed to collect structural data for trigonally distorted perovskites in specific model systems. Correlative models were developed which describe the relationship between the *c*/*a* ratio and the ratio of the pseudocubic lattice constant (a_{pc}) to the B-X bond length (r_{BX}). General models were then created for the *c*/*a* ratio in terms of the modified tolerance factor for trigonal perovskites with $R\bar{3}c$ symmetry and perovskite-like compounds with *R*3*c* symmetry. These models accurately predict the lattice constants in trigonally distorted perovskites and $LiNbO_3$ type perovskite-like compounds. In addition, a general model was developed, which accurately predicts polarization in trigonal $LiNbO_3$ type perovskite-like compounds in space group *R*3*c*.

KEYWORDS

electroceramics, modeling/model, perovskites, polarization

1 | INTRODUCTION

Correlative models describing composition-structure relationships are the keys to unlocking the full potential of many materials, including electroceramics. Perovskite ceramics exhibit an expansive range of properties, and examples of trigonally distorted perovskites alone exhibit colossal magnetoresistance (eg, $La_{0.6-x}Pr_xSr_{0.4}MnO_3$),[1] magnetocaloric effects (eg, $La_{0.65}Sr_{0.35}V_{0.1}Mn_{0.9}O_3$),[2] catalysis (eg, $La_{1-x}Ag_xMnO_3$),[3] and ferroelectricity (eg, $BiFeO_3$).[4] Thus, predictive models linking structure to properties are needed to minimize expensive and time-consuming trial-and-error experiments, allowing for a more cost-effective future for the electroceramics industry, with all the concomitant benefits for society which that entails.

Generally, perovskites are defined as compounds with ABX_3 stoichiometry in which large A-site cations exist on cuboctahedral sites between corner-sharing anion octahedra, each of which contains a smaller B-site cation. Trigonal distortion in perovskites occurs when the BO_6 octahedra undergo equal anti-phase octahedral tilting about all three crystallographic pseudocubic axes ($a^-a^-a^-$ in Glazer's notation[5]). This tilting results in the vast majority of trigonally distorted perovskites crystallizing in the centrosymmetric space group $R\bar{3}c$, although it is also possible for these perovskites to crystallize in the non-centrosymmetric space group *R*3*c*. Both $R\bar{3}c$ and *R*3*c* trigonal perovskites can be described with either a rhombohedral or hexagonal cell; however, a hexagonal cell is most often chosen for the sake of convenience; thus, all of the trigonally distorted perovskites in this work were considered in the hexagonal setting.

Additionally, the A site for all the trigonal perovskites that have been analyzed in this work contain a trivalent cation (eg, La^{3+}) and have been doped with either a divalent

TABLE 1 The 57 $R\bar{3}c$ trigonal compositions used to derive the general trigonal model for $c/a < \sqrt{6}$ (Figure 1)

ICSD #	Compound	$a_{pc\ (exptl.)}$ (Å)	$r_{B\text{-}X(exptl.)}$ (Å)	t' (Equation 3)	c/a_{exptl}	c/a_{calc}	|Error%|
98 069	$La_{0.6}Sr_{0.4}FeO_3$	3.8998	1.964	0.9868	2.4288	2.4269	0.0800
163 227	$La_{0.5}Sr_{0.5}FeO_3$	3.8889	1.954	0.9928	2.4343	2.4339	0.0161
78 067	$La_{0.4}Sr_{0.6}FeO_3$	3.8802	1.946	0.9992	2.4411	2.4397	0.0570
160 591	$La_{0.333}Sr_{0.667}FeO_3$	3.8733	1.938	1.0036	2.4491	2.4470	0.0851
190 643	$La_{0.33}Sr_{0.67}FeO_3$	3.8711	1.938	1.0038	2.4463	2.4452	0.0447
78 068	$La_{0.3}Sr_{0.7}FeO_3$	3.8715	1.937	1.0058	2.4479	2.4471	0.0342
Average systematic absolute error							0.0529
82 814	$La_{0.9}Sr_{0.1}CoO_3$	3.7756	1.901	0.9795	2.4225	2.4284	0.2435
164 487	$La_{0.85}Sr_{0.15}CoO_3$	3.8293	1.930	0.9830	2.4156	2.4247	0.3768
82 815	$La_{0.8}Sr_{0.2}CoO_3$	3.8029	1.913	0.9865	2.4247	2.4315	0.2837
156 454	$La_{0.7}Sr_{0.3}CoO_3$	3.8369	1.928	0.9937	2.4260	2.4354	0.3881
237 871	$La_{0.6}Sr_{0.4}CoO_3$	3.8344	1.926	1.0009	2.4306	2.4367	0.2542
93 380	$La_{0.5}Sr_{0.5}CoO_3$	3.8337	1.921	1.0082	2.4422	2.4453	0.1237
167 257	$LaCoO_3$	3.8243	1.932	0.9726	2.4056	2.4191	0.5607
Average systematic absolute error							0.3187
189 376	$La_{0.99}Ba_{0.01}CoO_3$	3.8265	1.929	0.9747	2.4138	2.4135	0.0091
157 894	$La_{0.97}Ba_{0.03}CoO_3$	3.8314	1.931	0.9789	2.4096	2.4145	0.2046
157 895	$La_{0.95}Ba_{0.05}CoO_3$	3.8356	1.933	0.9832	2.4123	2.4147	0.1013
157 896	$La_{0.92}Ba_{0.08}CoO_3$	3.8406	1.936	0.9896	2.4161	2.4138	0.0967
157 897	$La_{0.9}Ba_{0.1}CoO_3$	3.8447	1.936	0.9939	2.4188	2.4179	0.0374
157 898	$La_{0.88}Ba_{0.12}CoO_3$	3.8469	1.935	0.9982	2.4211	2.4220	0.0382
157 899	$La_{0.85}Ba_{0.15}CoO_3$	3.8518	1.936	1.0047	2.4247	2.4249	0.0062
157 900	$La_{0.82}Ba_{0.18}CoO_3$	3.8557	1.936	1.0111	2.4285	2.4287	0.0099
157 901	$La_{0.8}Ba_{0.2}CoO_3$	3.8585	1.936	1.0154	2.4310	2.4314	0.0162
157 902	$La_{0.75}Ba_{0.25}CoO_3$	3.8635	1.935	1.0261	2.4370	2.4383	0.0539
157 903	$La_{0.72}Ba_{0.28}CoO_3$	3.8666	1.936	1.0324	2.4410	2.4394	0.0643
157 904	$La_{0.7}Ba_{0.3}CoO_3$	3.8685	1.936	1.0365	2.4437	2.4413	0.0990
167 257	$LaCoO_3$	3.8243	1.932	0.9726	2.4056	2.4191	0.5607
Average systematic absolute error							0.0998
91 179	$La_{0.875}Ba_{0.125}MnO_3$	3.9095	1.973	0.9854	2.4187	2.4224	0.1522
91 180	$La_{0.85}Ba_{0.15}MnO_3$	3.9049	1.968	0.9897	2.4219	2.4257	0.1577
159 742	$La_{0.825}Ba_{0.175}MnO_3$	3.9328	1.981	0.9940	2.4288	2.4271	0.0718
91 182	$La_{0.8}Ba_{0.2}MnO_3$	3.9093	1.965	0.9986	2.4286	2.4323	0.1525
91 183	$La_{0.775}Ba_{0.225}MnO_3$	3.9094	1.966	1.0032	2.4301	2.4311	0.0380
91 184	$La_{0.75}Ba_{0.25}MnO_3$	3.9081	1.965	1.0079	2.4324	2.4315	0.0359
82 104	$La_{0.7}Ba_{0.3}MnO_3$	3.9097	1.962	1.0175	2.4380	2.4363	0.0690
185 842	$La_{0.67}Ba_{0.33}MnO_3$	3.9073	1.958	1.0235	2.4409	2.4398	0.0425
96 038	$LaMnO_3$	3.8705	1.960	0.9667	2.4135	2.4163	0.1161
Average systematic absolute error							0.0929
97 865	$La_{0.82}Sr_{0.18}MnO_3$	3.8924	1.969	0.9754	2.4159	2.4127	0.1354
97 866	$La_{0.8}Sr_{0.2}MnO_3$	3.8899	1.967	0.9765	2.4175	2.4140	0.1453
162 762	$La_{0.7}Sr_{0.3}MnO_3$	3.8812	1.955	0.9826	2.4268	2.4278	0.0407
160 750	$La_{0.67}Sr_{0.33}MnO_3$	3.8853	1.956	0.9848	2.4290	2.4297	0.0286

(Continues)

TABLE 1 (Continued)

ICSD #	Compound	$a_{pc\ (exptl.)}$ (Å)	$r_{B\text{-}X(exptl.)}$ (Å)	t' (Equation 3)	c/a exptl	c/a calc	|Error%|
95 568	$La_{0.64}Sr_{0.36}MnO_3$	3.8805	1.954	0.9867	2.4290	2.4290	0.0026
99 555	$La_{0.6}Sr_{0.4}MnO_3$	3.8708	1.944	0.9895	2.4359	2.4384	0.1012
236 939	$La_{0.55}Sr_{0.45}MnO_3$	3.8656	1.940	0.9932	2.4372	2.4410	0.1541
96 038	$LaMnO_3$	3.8705	1.960	0.9667	2.4135	2.4163	0.1161
Average systematic absolute error							0.0905
155 413	$La_{0.95}Ca_{0.05}MnO_3$	3.8873	1.967	0.9661	2.4158	2.4204	0.1904
238 369	$La_{0.8}Ca_{0.2}MnO_3$	3.8784	1.959	0.9644	2.4347	2.4384	0.1548
161 685	$La_{0.7}Ca_{0.3}MnO_3$	3.8676	1.953	0.9633	2.4436	2.4412	0.0977
258 206	$La_{0.6}Ca_{0.4}MnO_3$	3.8637	1.952	0.9623	2.4418	2.4361	0.2312
96 038	$LaMnO_3$	3.8705	1.960	0.9667	2.4135	2.4163	0.1161
Average systematic absolute error							0.1580
257 499	$La_{0.9}Na_{0.1}MnO_3$	3.8761	1.955	0.9685	2.4202	2.4213	0.0457
161 362	$La_{0.67}Na_{0.33}MnO_3$	3.8711	1.939	0.9772	2.4254	2.4299	0.1871
96 038	$LaMnO_3$	3.8705	1.960	0.9667	2.4135	2.4163	0.1161
Average systematic absolute error							0.1163
185 478	$La_{0.9}K_{0.1}MnO_3$	3.8938	1.964	0.9842	2.4222	2.4177	0.1869
185 479	$La_{0.875}K_{0.125}MnO_3$	3.8928	1.960	0.9893	2.4221	2.4210	0.0460
185 480	$La_{0.85}K_{0.15}MnO_3$	3.8884	1.957	0.9948	2.4249	2.4217	0.1299
96 038	$LaMnO_3$	3.8705	1.960	0.9667	2.4135	2.4163	0.1161
Average systematic absolute error							0.1197
168 695	$La_{0.95}Ag_{0.05}MnO_3$	3.8809	1.958	0.9698	2.4222	2.4201	0.0879
168 696	$La_{0.9}Ag_{0.1}MnO_3$	3.8801	1.958	0.9735	2.4233	2.4196	0.1523
241 662	$La_{0.85}Ag_{0.15}MnO_3$	3.8899	1.964	0.9778	2.4218	2.4183	0.1420
153 552	$La_{0.8}Ag_{0.2}MnO_3$	3.8729	1.953	0.9826	2.4268	2.4212	0.2301
96 038	$LaMnO_3$	3.8705	1.960	0.9667	2.4135	2.4163	0.1161
Average systematic absolute error							0.1457
96 039	$La_{0.9}Pb_{0.1}MnO_3$	3.8733	1.957	0.9788	2.4155	2.4140	0.0593
167 676	$La_{0.67}Pb_{0.33}MnO_3$	3.9116	1.956	1.0041	2.4429	2.4241	0.7683
95 498	$La_{0.65}Pb_{0.35}MnO_3$	3.8795	1.955	1.0064	2.4225	2.4166	0.2435
96 038	$LaMnO_3$	3.8705	1.960	0.9667	2.4135	2.4163	0.1161
Average systematic absolute error							0.2968
Global average absolute error							0.1348

cation (eg, Sr^{2+}) or a monovalent cation (eg, Na^{+}) according to the following stoichiometries: $A^{3+}_{1-x}A^{2+}_{x}B^{3+}_{1-x}B^{4+}_{x}O_3$ or $A^{3+}_{1-x/2}A^{1+}_{x/2}B^{3+}_{1-x}B^{4+}_{x}O_3$. Using these formulas, a divalent cation species can completely replace the trivalent one ($x = 1$) without the need for oxygen vacancies for charge compensation; however, a monovalent A-site dopant can only be used to replace half of the trivalent one before intrinsic oxygen vacancies or second phases would begin to form.

Many of the trigonal perovskites that have been produced to date contain manganese on the B site due to its useful magnetic properties. Mn^{3+} is a well-known Jahn-Teller ion, and the Mn^{3+} cation is known to exist purely in its high-spin (HS) state $\left(t^3_{2g}e^1_g\right)$ at room temperature and atmospheric pressure.[6] Furthermore, the Mn^{3+} cation is well known for its ability to change oxidation states, which allows for series such as $LnMnO_3$ to be doped with divalent or monovalent cations while maintaining fully occupied anion sites. For instance, doping $LaMnO_3$ with a quantity of Sr^{2+} causes the formation of an equal amount of Mn^{4+}. Interestingly, electrons can migrate between Mn^{3+} and Mn^{4+} cations via the double exchange mechanism; thus, if the dopant reaches sufficient concentration (ie, the Mn^{4+} concentration reaches sufficient concentration), it can cause the electrons to delocalize from these cations and allow the sample to exhibit metallic conductivity.[6]

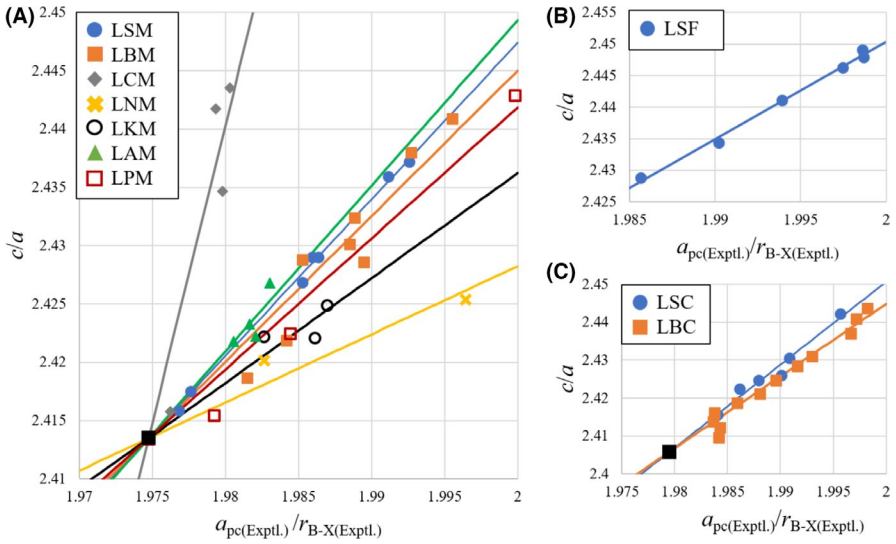

FIGURE 1 Linear fits describing c/a vs $a_{pc(Exptl.)}/r_{BX(Exptl.)}$ for the (A) $La^{3+}_{1-x}A^{2+}_{x}Mn^{3+}_{1-x}Mn^{4+}_{x}O_3$, $La^{3+}_{1-x}A^{1+}_{x}Mn^{3+}_{1-2x}Mn^{4+}_{2x}O_3$, (B) $La^{3+}_{1-x}A^{2+}_{x}Fe^{3+}_{1-x}Fe^{4+}_{x}O_3$, and (C) $La^{3+}_{1-x}A^{2+}_{x}Co^{3+}_{1-x}Co^{4+}_{x}O_3$ systems [Color figure can be viewed at wileyonlinelibrary.com]

On the other hand, the spin state of the Co^{3+} cation in the $LnCoO_3$ series of compounds is a bit ambiguous. Current research[6] suggests that Co^{3+} exists in its low-spin (LS) state $\left(t^6_{2g}\right)$ at room temperature and atmospheric pressure but transitions to an intermediate-spin (IS) state $\left(t^5_{2g}e^1_g\right)$ at higher temperatures and pressures. Furthermore, Fe^{3+} is known to exist purely in its high-spin state $\left(t^3_{2g}e^2_g\right)$ at room temperature and atmospheric pressure.[7] Thus, for the sake of choosing the appropriate ionic radii, Mn^{3+} and Fe^{3+} were considered in their high-spin states and Co^{3+} was considered in its low-spin state for the perovskites in this work.

There currently exist several correlative models for predicting both cubic[8-10] and orthorhombic[11,12] perovskite lattice parameters. There even exists an empirical model for predicting tetragonal lattice parameters in perovskites[13]; however, there are currently no empirical models for predicting lattice constants in trigonally distorted perovskites, arguably a larger and more commercially relevant class of perovskite.

In 2001, Lufaso and Woodward developed[14] a program called SPuDS (Structure Prediction Diagnostic Software) for predicting perovskite structures. It was based on the concept of the global-instability-index (GII) as developed by Salinas-Sanchez et al.[15] SPuDS is a very powerful tool, and it is currently one of the only methods available for predicting the stability of trigonal perovskites; however, because SPuDS relies solely on the GII, it cannot unambiguously predict the most stable perovskite structures in many cases. It also fails to account for B-site octahedral distortions and does not account for some atomic species (eg, Pm^{3+} and Ra^{2+}).

The first method ever developed for predicting the perovskite stability was Goldschmidt's tolerance factor,[16] which is defined as the following:

$$t_0 = \frac{\left(r_A + r_X\right)}{\sqrt{2}\left(r_B + r_X\right)}, \tag{1}$$

where r_A, r_B, and r_X are the Shannon[17] radii of the A, B, and X species, respectively. The experimental pseudocubic lattice constant can be defined using experimental parameters as:

$$a_{pc(Exptl.)} = \left(\frac{V}{Z}\right)^{1/3}, \tag{2}$$

where V is the unit-cell volume and Z is the number of ABX_3 formula units per unit cell.

Recently, Bartel et al[18] developed a new model for predicting the perovskite tolerance factor, which requires the oxidation number and Shannon radii of each species as input. This model significantly improves upon the accuracy of the Goldschmidt's tolerance factor; however, this model does not use the ionic radii of each species in their correct coordination environments. Instead, it requires the radii of A, B, and X ions to be in sixfold coordination. On the other hand, Ubic et al[10,19-21] have recently developed a model for the tolerance factor, t', that does account for the A, B, and X ions in their correct coordinations (XII, VI, and II, respectively):

$$t' = \frac{a_{pc} - 0.011730139}{0.7209203\left(r_B + r_X\right)} - 1.760998, \tag{3}$$

where a_{pc} is determined either experimentally or via an empirical model.[22] Additionally, this model accounts for A-site vacancies among other extrinsic defects, and has been proven[22] to be much more effective than Goldschmidt's tolerance factor at predicting the tilt structures and pseudocubic lattice constants of perovskites. This model has also recently been extended to account for the effects of A-site[23] and B-site[24] ordering. The pseudocubic lattice constant, a_{pc}, can be defined in two ways according to this model:

$$a'_{pc} = \sqrt{2}\left(r_A + r_X\right), \tag{4}$$

TABLE 2 Experimental and calculated trigonal lattice constants from Equation 10, 11, and 13 for the 57 $R\bar{3}c$ trigonal compositions

ICSD #	Compound	$a_{(Exptl.)}$ (Å)	$a_{(Calc.)}$ (Å)	|Error%|	$c_{(Exptl.)}$ (Å)	$c_{(Calc.)}$ (Å)	|Error%|
98 069	$La_{0.6}Sr_{0.4}FeO_3$	5.5308	5.5323	0.0267	13.4334	13.4262	0.0533
163 227	$La_{0.5}Sr_{0.5}FeO_3$	5.5111	5.5114	0.0054	13.4158	13.4143	0.0108
78 067	$La_{0.4}Sr_{0.6}FeO_3$	5.4937	5.4947	0.0190	13.4106	13.4055	0.0380
160 591	$La_{0.33}Sr_{0.67}FeO_3$	5.4780	5.4796	0.0284	13.4160	13.4084	0.0568
190 643	$La_{0.33}Sr_{0.67}FeO_3$	5.4769	5.4777	0.0149	13.3980	13.3940	0.0298
78 068	$La_{0.3}Sr_{0.7}FeO_3$	5.4762	5.4769	0.0114	13.4055	13.4025	0.0228
Average systematic absolute error		0.0176			0.0352		
82 814	$La_{0.9}Sr_{0.1}CoO_3$	5.3594	5.3550	0.0810	12.9828	13.0039	0.1623
164 487	$La_{0.85}Sr_{0.15}CoO_3$	5.4406	5.4338	0.1253	13.1423	13.1753	0.2511
82 815	$La_{0.8}Sr_{0.2}CoO_3$	5.3964	5.3913	0.0944	13.0844	13.1092	0.1890
156 454	$La_{0.7}Sr_{0.3}CoO_3$	5.4437	5.4367	0.1290	13.2062	13.2404	0.2586
237 871	$La_{0.6}Sr_{0.4}CoO_3$	5.4367	5.4321	0.0846	13.2142	13.2366	0.1694
93 380	$La_{0.5}Sr_{0.5}CoO_3$	5.4270	5.4248	0.0412	13.2540	13.2649	0.0825
167 257	$LaCoO_3$	5.4410	5.4309	0.1862	13.0890	13.1379	0.3734
Average systematic absolute error		0.1060			0.2123		
189 376	$La_{0.99}Ba_{0.01}CoO_3$	5.4380	5.4382	0.0030	13.1260	13.1252	0.0061
157 894	$La_{0.97}Ba_{0.03}CoO_3$	5.4482	5.4445	0.0681	13.1280	13.1459	0.1364
157 895	$La_{0.95}Ba_{0.05}CoO_3$	5.4521	5.4503	0.0338	13.1520	13.1609	0.0675
157 896	$La_{0.92}Ba_{0.08}CoO_3$	5.4563	5.4581	0.0323	13.1830	13.1745	0.0645
157 897	$La_{0.9}Ba_{0.1}CoO_3$	5.4602	5.4609	0.0125	13.2070	13.2037	0.0249
157 898	$La_{0.88}Ba_{0.12}CoO_3$	5.4616	5.4609	0.0127	13.2230	13.2264	0.0255
157 899	$La_{0.85}Ba_{0.15}CoO_3$	5.4658	5.4657	0.0021	13.2530	13.2536	0.0041
157 900	$La_{0.82}Ba_{0.18}CoO_3$	5.4685	5.4683	0.0033	13.2800	13.2809	0.0066
157 901	$La_{0.8}Ba_{0.2}CoO_3$	5.4705	5.4702	0.0054	13.2990	13.3004	0.0108
157 902	$La_{0.75}Ba_{0.25}CoO_3$	5.4731	5.4721	0.0180	13.3380	13.3428	0.0360
157 903	$La_{0.72}Ba_{0.28}CoO_3$	5.4745	5.4757	0.0214	13.3630	13.3573	0.0428
157 904	$La_{0.7}Ba_{0.3}CoO_3$	5.4752	5.4757	0.0330	13.3800	13.3712	0.0660
167 257	$LaCoO_3$	5.4410	5.4309	0.1862	13.0890	13.1379	0.3734
Average systematic absolute error		0.0332			0.0665		
91 179	$La_{0.875}Ba_{0.125}MnO_3$	5.5522	5.5494	0.0507	13.4290	13.4426	0.1014
91 180	$La_{0.85}Ba_{0.15}MnO_3$	5.5432	5.5403	0.0525	13.4250	13.4391	0.1051
159 742	$La_{0.825}Ba_{0.175}MnO_3$	5.5776	5.5789	0.0240	13.5470	13.5405	0.0479
91 182	$La_{0.8}Ba_{0.2}MnO_3$	5.5444	5.5416	0.0508	13.4650	13.4787	0.1017
91 183	$La_{0.775}Ba_{0.225}MnO_3$	5.5433	5.5426	0.0126	13.4710	13.4744	0.0253
91 184	$La_{0.75}Ba_{0.25}MnO_3$	5.5398	5.5405	0.0120	13.4750	13.4718	0.0239
82 104	$La_{0.7}Ba_{0.3}MnO_3$	5.5378	5.5391	0.0230	13.5011	13.4949	0.0460
185 842	$La_{0.67}Ba_{0.33}MnO_3$	5.5322	5.5330	0.0142	13.5034	13.4996	0.0283
96 038	$LaMnO_3$	5.5008	5.4987	0.0387	13.2760	13.2863	0.0774
Average systematic absolute error		0.0309			0.0619		
97 865	$La_{0.82}Sr_{0.18}MnO_3$	5.5300	5.5325	0.0452	13.3600	13.3480	0.0903
97 866	$La_{0.8}Sr_{0.2}MnO_3$	5.5253	5.5280	0.0485	13.3577	13.3448	0.0969

(Continues)

TABLE 2 (Continued)

ICSD #	Compound	$a_{(Exptl.)}$ (Å)	$a_{(Calc.)}$ (Å)	|Error%|	$c_{(Exptl.)}$ (Å)	$c_{(Calc.)}$ (Å)	|Error%|
162 762	$La_{0.7}Sr_{0.3}MnO_3$	5.5059	5.5052	0.0135	13.3619	13.3655	0.0271
160 750	$La_{0.667}Sr_{0.333}MnO_3$	5.5100	5.5095	0.0095	13.3840	13.3866	0.0191
95 568	$La_{0.64}Sr_{0.36}MnO_3$	5.5032	5.5032	0.0009	13.3675	13.3673	0.0017
99 555	$La_{0.6}Sr_{0.4}MnO_3$	5.4843	5.4825	0.0337	13.3594	13.3684	0.0675
236 939	$La_{0.55}Sr_{0.45}MnO_3$	5.4760	5.4732	0.0513	13.3461	13.3598	0.1027
96 038	$LaMnO_3$	5.5008	5.4987	0.0387	13.2760	13.2863	0.0774
Average systematic absolute error		0.0302			0.0603		
155 413	$La_{0.95}Ca_{0.05}MnO_3$	5.5229	5.5194	0.0634	13.3420	13.3589	0.1269
238 369	$La_{0.8}Ca_{0.2}MnO_3$	5.4960	5.4932	0.0515	13.3810	13.3948	0.1031
161 685	$La_{0.7}Ca_{0.3}MnO_3$	5.4740	5.4758	0.0326	13.3760	13.3673	0.0652
258 206	$La_{0.6}Ca_{0.4}MnO_3$	5.4698	5.4740	0.0772	13.3559	13.3353	0.1542
96 038	$LaMnO_3$	5.5008	5.4987	0.0387	13.2760	13.2863	0.0774
Average systematic absolute error		0.0527			0.1054		
257 499	$La_{0.9}Na_{0.1}MnO_3$	5.5037	5.5029	0.0152	13.3199	13.3240	0.0304
161 362	$La_{0.67}Na_{0.33}MnO_3$	5.4926	5.4892	0.0623	13.3217	13.3383	0.1247
96 038	$LaMnO_3$	5.5008	5.4987	0.0387	13.2760	13.2863	0.0774
Average systematic absolute error		0.0387			0.0775		
185 478	$La_{0.9}K_{0.1}MnO_3$	5.5273	5.5307	0.0624	13.3883	13.3716	0.1246
185 479	$La_{0.875}K_{0.125}MnO_3$	5.5259	5.5267	0.0153	13.3842	13.3801	0.0306
185 480	$La_{0.85}K_{0.15}MnO_3$	5.5176	5.5200	0.0434	13.3796	13.3680	0.0866
96 038	$LaMnO_3$	5.5008	5.4987	0.0387	13.2760	13.2863	0.0774
Average systematic absolute error		0.0399			0.0798		
168 695	$La_{0.95}Ag_{0.05}MnO_3$	5.5090	5.5106	0.0293	13.3440	13.3362	0.0586
168 696	$La_{0.9}Ag_{0.1}MnO_3$	5.5070	5.5098	0.0508	13.3450	13.3315	0.1015
241 662	$La_{0.85}Ag_{0.15}MnO_3$	5.5220	5.5246	0.0474	13.3730	13.3603	0.0947
153 552	$La_{0.8}Ag_{0.2}MnO_3$	5.4941	5.4984	0.0768	13.3332	13.3127	0.1535
96 038	$LaMnO_3$	5.5008	5.4987	0.0387	13.2760	13.2863	0.0774
Average systematic absolute error		0.0486			0.0971		
96 039	$La_{0.9}Pb_{0.1}MnO_3$	5.5033	5.5044	0.0198	13.2930	13.2877	0.0395
167 676	$La_{0.67}Pb_{0.33}MnO_3$	5.5368	5.5511	0.2574	13.5258	13.4564	0.5129
95 498	$La_{0.65}Pb_{0.35}MnO_3$	5.5068	5.5113	0.0813	13.3401	13.3184	0.1624
96 038	$LaMnO_3$	5.5008	5.4987	0.0387	13.2760	13.2863	0.0774
Average systematic absolute error		0.0993			0.1981		
Global average absolute error		0.0449			0.0898		

$$a''_{pc} = 2\left(r_B + r_X\right), \tag{5}$$

The keys to this model are the concepts that the effective r_X is a function of t_0 and that the effective r_A is a function of both A-site vacancy concentration, x, and t_0, which can now be redefined[22] as the ratio of Equations (4) and (5):

$$t_0 = \frac{a'_{pc}}{a''_{pc}} = \frac{\left(r_A + r_X\right)}{\sqrt{2}\left(r_B + r_X\right)}. \tag{6}$$

TABLE 3 Coefficients of Equation 7

Composition	*A*	*B*	R^2
$La_{1-x}Sr_xFeO_3$	1.543171	−0.635964	0.9937
$La_{1-x}Sr_xCoO_3$	2.191690	−1.932677	0.9809
$La_{1-x}Ba_xCoO_3$	1.907794	−1.370724	0.9728
$La_{1-x}Sr_xMnO_3$	1.343478	−0.239554	0.9977
$La_{1-x}Ba_xMnO_3$	1.249331	−0.053637	0.9273
$La_{1-x}Ca_xMnO_3$	5.104347	−7.666295	0.9075
$La_{1-x}Na_xMnO_3$	0.584690	1.258855	0.9320
$La_{1-x}K_xMnO_3$	0.900957	0.634310	0.9244
$La_{1-x}Ag_xMnO_3$	1.420578	−0.391807	0.9464
$La_{1-x}Pb_xMnO_3$	1.124310	0.193246	0.9737

2 | MATERIALS AND METHODS

In this work, 57 trigonally distorted perovskites in space group $R\bar{3}c$ and 31 trigonally distorted perovskites in space group $R3c$ were mined from literature. A total of 10 compositional series were analyzed for the perovskites in space group $R\bar{3}c$: $La_{1-x}Sr_xFeO_3$ (LSF), $La_{1-x}Sr_xCoO_3$ (LSC), $La_{1-x}Ba_xCoO_3$ (LBC), $La_{1-x}Sr_xMnO_3$ (LSM), $La_{1-x}Ba_xMnO_3$ (LBM), $La_{1-x}Ca_xMnO_3$ (LCM), $La_{1-x}Na_xMnO_3$ (LNM), $La_{1-x}K_xMnO_3$ (LKM), $La_{1-x}Ag_xMnO_3$ (LAM), and $La_{1-x}Pb_xMnO_3$ (LPM). Using the data from these perovskites, system-specific models were developed for the perovskites in space group $R\bar{3}c$ which describe the *c*/*a* ratio as a function of the ratio of the pseudocubic lattice constant to the B-X bond length. From the system-specific models, a general model describing perovskite trigonality for perovskites in space group $R\bar{3}c$ in terms of the modified tolerance factor[19] was derived. In addition, a general model was developed for both trigonality and intrinsic polarization in $LiNbO_3$ type structures with space group $R3c$.

3 | RESULTS AND DISCUSSION

Table 1 shows the data for all 57 compounds used to derive the general trigonal model for perovskites with $R\bar{3}c$ symmetry and the predicted perovskite trigonality, *c*/*a*, using this model. Values of t' were determined from an empirical model[22] using only the values of t_0 and Shannon[17] values of r_A for each compound. Additionally, Table 1 shows the average systematic absolute errors, which is the average of the absolute errors, for each trigonal system, and the average global absolute error for all the trigonal systems combined. After applying the trigonal model to each compound, the average global absolute error between the experimental and predicted *c*/*a* values is 0.1348%.

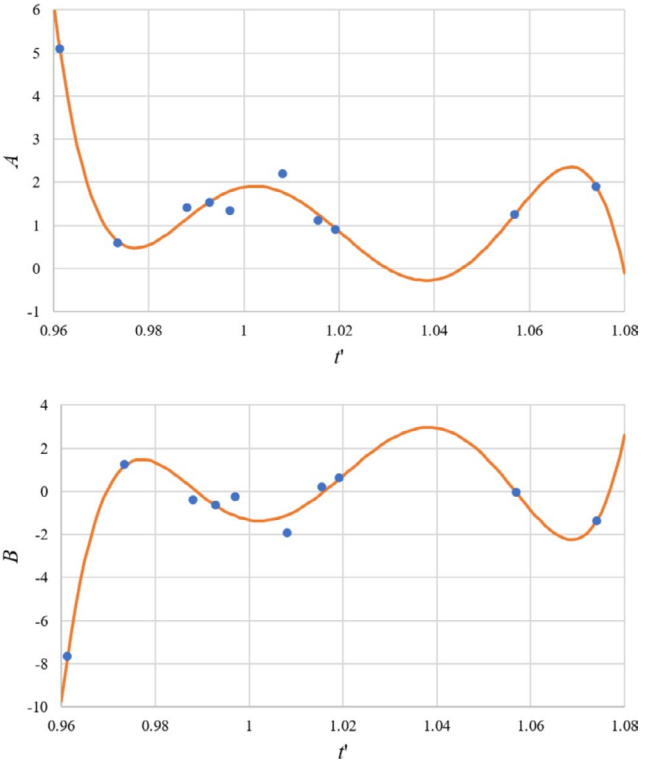

FIGURE 2 Coefficients of Equation 7 vs tolerance factor[22] [Color figure can be viewed at wileyonlinelibrary.com]

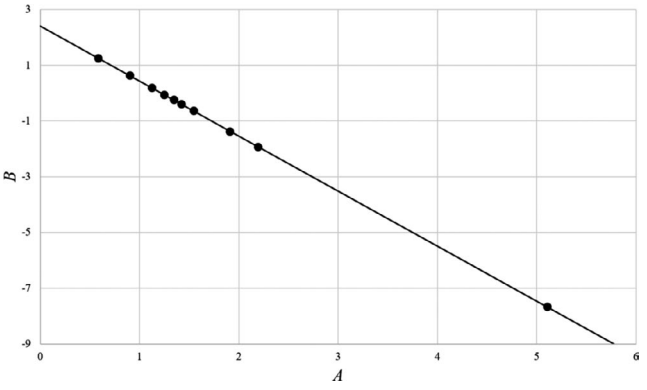

FIGURE 3 Linear correlation between the coefficients of Equation 7

TABLE 4 Coefficients of Equation 8

Coefficients	*a* (×10⁸)	*b* (×10⁸)	*c* (×10⁸)	*d* (×10⁸)	*e* (×10⁸)	*f* (×10⁸)	R^2
A	−0.27959879	1.42820323	−2.91700005	2.97772686	−1.51927238	0.30994115	0.9674
B	0.55247258	−2.82207672	5.76392731	−5.88396483	3.00209134	−0.61244969	0.9669

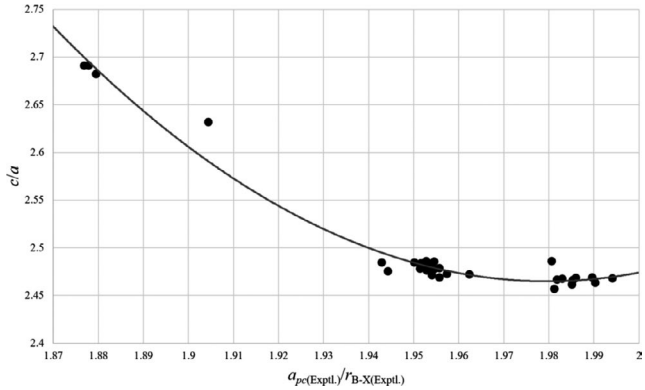

FIGURE 4 Quadratic fit describing c/a vs $a_{pc(Exptl.)}/r_{BX(Exptl.)}$ for the 31 $R3c$ trigonal compositions

The two systems producing the most error are $La_{1-x}Sr_xCoO_3$ (0.3187%) and $La_{1-x}Pb_xMnO_3$ (0.2968%), whereas the system producing the least amount of error is $La_{1-x}Sr_xFeO_3$ (0.0529%).

Table 2 shows the experimental and predicted trigonal lattice constants using Equations 10-13 for all 57 $R\bar{3}c$ trigonal compounds used in this model. The average global absolute error for a and c is 0.0449% and 0.0898%, respectively. Again, the two systems producing the most error are $La_{1-x}Sr_xCoO_3$ (0.1060% for a and 0.2123% for c) and $La_{1-x}Pb_xMnO_3$ (0.0993% for a and 0.1981% for c), and the system producing the least amount of error is $La_{1-x}Sr_xFeO_3$ (0.0176% for a and 0.0352% for c). It should be noted that the errors are very good overall; however, one of the reasons that the $La_{1-x}Pb_xMnO_3$ compound has the largest errors may be due to the fact that Pb

TABLE 5 The 31 $R3c$ trigonal compositions used to derive the general trigonal model for $c/a > \sqrt{6}$ (Figure 4)

ICSD #	Compound	$a_{pc(Exptl.)}$ (Å)	$r_{B-X(Exptl.)}$ (Å)	c/a Exptl	c/a Calc	|Error%|
250 775	$LiNbO_3$	3.9651	2.002	2.4862	2.4648	0.8585
35 012	$LiReO_3$	3.6879	1.937	2.6323	2.5907	1.5779
98 123	$(Li_{0.937}Zn_{0.063})(Nb_{0.979}Zn_{0.021})O_3$	3.7602	2.004	2.6913	2.6999	0.3177
98 125	$(Li_{0.94}Zn_{0.06})(Nb_{0.98}Zn_{0.02})O_3$	3.7602	2.003	2.6913	2.6956	0.1592
250 774	$Li_{0.96}Na_{0.04}NbO_3$	3.7645	2.003	2.6824	2.6882	0.2159
280 368	$PbHf_{0.8}Ti_{0.2}O_3$	4.1050	2.063	2.4635	2.4673	0.1543
46 024	$PbZr_{0.9}Ti_{0.1}O_3$	4.1406	2.077	2.4681	2.4694	0.0526
86 131	$PbZr_{0.871}Ti_{0.129}O_3$	4.1432	2.087	2.4663	2.4655	0.0327
86 132	$PbZr_{0.838}Ti_{0.162}O_3$	4.1370	2.087	2.4670	2.4649	0.0837
86 133	$PbZr_{0.796}Ti_{0.204}O_3$	4.1282	2.082	2.4678	2.4650	0.1102
86 134	$PbZr_{0.745}Ti_{0.255}O_3$	4.1213	2.075	2.4684	2.4657	0.1118
86 135	$PbZr_{0.7}Ti_{0.3}O_3$	4.1128	2.067	2.4691	2.4670	0.0850
237 367	$BiFeO_3$	3.9651	2.031	2.4862	2.4809	0.2103
193 811	$Bi_{0.5}Na_{0.5}TiO_3$	3.8870	1.962	2.4569	2.4648	0.3250
237 369	$BiFe_{0.8}Co_{0.2}O_3$	3.9436	2.017	2.4788	2.4776	0.0491
261 637	$Bi_{0.95}Tb_{0.05}FeO_3$	3.9587	2.029	2.4837	2.4824	0.0538
261 638	$Bi_{0.9}Tb_{0.1}FeO_3$	3.9587	2.029	2.4837	2.4824	0.0538
261 639	$Bi_{0.85}Tb_{0.15}FeO_3$	3.9484	2.023	2.4807	2.4821	0.0568
182 003	$Bi_{0.88}Sm_{0.12}FeO_3$	3.9535	2.026	2.4781	2.4826	0.1796
194 413	$Bi_{0.9}La_{0.1}FeO_3$	3.9585	2.036	2.4754	2.4927	0.7007
181 565	$Bi_{0.815}La_{0.185}FeO_3$	3.9465	2.018	2.4693	2.4776	0.3382
193 639	$BiFe_{0.98}Co_{0.02}O_3$	3.9655	2.029	2.4855	2.4790	0.2631
82 615	$Bi_{0.93}La_{0.07}FeO_3$	3.9554	2.026	2.4765	2.4809	0.1759
51 662	$BiFe_{0.8}Mn_{0.2}O_3$	3.9559	2.024	2.4780	2.4789	0.0367
51 663	$BiFe_{0.9}Mn_{0.1}O_3$	3.9624	2.029	2.4834	2.4802	0.1289
192 514	$Bi_{0.95}Dy_{0.05}FeO_3$	3.9596	2.031	2.4848	2.4843	0.0208
165 908	$Bi_{0.85}La_{0.15}FeO_3$	3.9596	2.038	2.4848	2.4949	0.4056
187 231	$Bi_{0.87}La_{0.13}FeO_3$	3.9577	2.022	2.4728	2.4759	0.1259
188 046	$BiFe_{0.9}Ti_{0.1}O_3$	3.9580	2.017	2.4721	2.4715	0.0234
252 624	$Bi_{0.9}Pb_{0.1}FeO_3$	3.9583	1.994	2.4619	2.4654	0.1451
163 686	$Bi_{0.9}Ca_{0.1}FeO_3$	3.9481	2.021	2.4714	2.4794	0.3251
Average absolute error						0.2380

TABLE 6 Experimental and calculated trigonal lattice constants from Equations 12 and 13 for the 31 *R*3*c* trigonal compositions

ICSD #	Compound	$a_{(Exptl.)}$ (Å)	$a_{(Calc.)}$ (Å)	|Error%|	$c_{(Exptl.)}$ (Å)	$c_{(Calc.)}$ (Å)	|Error%|
250 775	$LiNbO_3$	5.5797	5.5958	0.2878	13.8721	13.7926	0.5731
35 012	$LiReO_3$	5.0918	5.1189	0.5316	13.4030	13.2616	1.0547
98 123	$(Li_{0.937}Zn_{0.063})(Nb_{0.979}Zn_{0.021})O_3$	5.1534	5.1480	0.1057	13.8696	13.8990	0.2117
98 125	$(Li_{0.94}Zn_{0.06})(Nb_{0.98}Zn_{0.02})O_3$	5.1534	5.1507	0.0530	13.8696	13.8843	0.1061
250 774	$Li_{0.96}Na_{0.04}NbO_3$	5.1650	5.1613	0.0719	13.8545	13.8744	0.1439
280 368	$PbHf_{0.8}Ti_{0.2}O_3$	5.7943	5.7913	0.0514	14.2742	14.2889	0.1029
46 024	$PbZr_{0.9}Ti_{0.1}O_3$	5.8410	5.8400	0.0175	14.4160	14.4211	0.0351
86 131	$PbZr_{0.871}Ti_{0.129}O_3$	5.8461	5.8467	0.0109	14.4182	14.4151	0.0218
86 132	$PbZr_{0.838}Ti_{0.162}O_3$	5.8367	5.8383	0.0279	14.3989	14.3909	0.0558
86 133	$PbZr_{0.796}Ti_{0.204}O_3$	5.8238	5.8259	0.0368	14.3716	14.3610	0.0735
86 134	$PbZr_{0.745}Ti_{0.255}O_3$	5.8134	5.8156	0.0373	14.3500	14.3393	0.0746
86 135	$PbZr_{0.7}Ti_{0.3}O_3$	5.8010	5.8026	0.0283	14.3230	14.3149	0.0567
237 367	$BiFeO_3$	5.5797	5.5836	0.0702	13.8721	13.8526	0.1403
193 811	$Bi_{0.5}Na_{0.5}TiO_3$	5.4916	5.4857	0.1081	13.4921	13.5213	0.2165
237 369	$BiFe_{0.8}Co_{0.2}O_3$	5.5551	5.5560	0.0164	13.7700	13.7655	0.0328
261 637	$Bi_{0.95}Tb_{0.05}FeO_3$	5.5726	5.5737	0.0179	13.8409	13.8359	0.0359
261 638	$Bi_{0.9}Tb_{0.1}FeO_3$	5.5726	5.5737	0.0179	13.8409	13.8359	0.0359
261 639	$Bi_{0.85}Tb_{0.15}FeO_3$	5.5603	5.5593	0.0189	13.7937	13.7989	0.0379
182 003	$Bi_{0.88}Sm_{0.12}FeO_3$	5.5695	5.5662	0.0598	13.8020	13.8185	0.1197
194 413	$Bi_{0.9}La_{0.1}FeO_3$	5.5786	5.5656	0.2325	13.8090	13.8734	0.4666
181 565	$Bi_{0.815}La_{0.185}FeO_3$	5.5663	5.5600	0.1125	13.7447	13.7757	0.2254
193 639	$BiFe_{0.98}Co_{0.02}O_3$	5.5809	5.5858	0.0879	13.8714	13.8471	0.1755
82 615	$Bi_{0.93}La_{0.07}FeO_3$	5.5734	5.5701	0.0586	13.8025	13.8187	0.1172
51 662	$BiFe_{0.8}Mn_{0.2}O_3$	5.5729	5.5722	0.0122	13.8097	13.8131	0.0245
51 663	$BiFe_{0.9}Mn_{0.1}O_3$	5.5780	5.5804	0.0430	13.8525	13.8406	0.0860
192 514	$Bi_{0.95}Dy_{0.05}FeO_3$	5.5730	5.5734	0.0069	13.8480	13.8461	0.0138
165 908	$Bi_{0.85}La_{0.15}FeO_3$	5.5730	5.5655	0.1348	13.8480	13.8854	0.2702
187 231	$Bi_{0.87}La_{0.13}FeO_3$	5.5793	5.5770	0.0419	13.7967	13.8083	0.0839
188 046	$BiFe_{0.9}Ti_{0.1}O_3$	5.5804	5.5808	0.0078	13.7951	13.7930	0.0156
252 624	$Bi_{0.9}Pb_{0.1}FeO_3$	5.5885	5.5858	0.0483	13.7582	13.7715	0.0967
163 686	$Bi_{0.9}Ca_{0.1}FeO_3$	5.5670	5.5609	0.1081	13.7581	13.7879	0.2166
Average absolute error				0.0795			0.1587

is volatile during the calcination and sintering stages of processing. Thus, if care is not taken to minimize the amount of lead loss in these compounds, it can cause oxygen vacancies and/or multiple phases to form.

Figure 1 shows the relationship between *c*/*a* and the ratio of the pseudocubic lattice constant, a_{pc}, to the B-X bond length, r_{BX}. These fits show that this trend is linear so can be represented by Equation 7:

$$\frac{c}{a} = A\left(\frac{a_{pc}}{r_{BX}}\right) + B, \tag{7}$$

Figure 1 also shows that the seven series with Mn on the B site clearly converge at $LaMnO_3$ and the two series with Co on the B site converge at $LaCoO_3$. Table 3 shows all of the coefficients and the goodness of fits for the trends represented by Equation 7.

Figure 2 demonstrates the relationship between the modified tolerance factor[22] and the coefficients of Equation 7. Both coefficients of Equation 7 (*A* and *B*) can be represented by the same fifth-order polynomial as a function of t', which is the minimum order polynomial that fits the data:

$$\text{Coeff} = at'^5 + bt'^4 + ct'^3 + dt'^2 + et' + f, \tag{8}$$

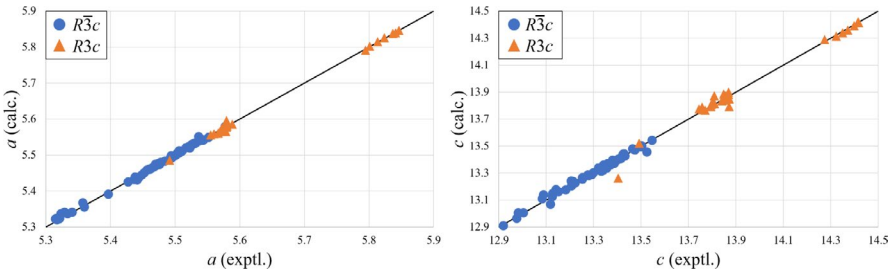

FIGURE 5 Predicted trigonal lattice constants of all 72 trigonally distorted perovskites and 31 $LiNbO_3$ type structures [Color figure can be viewed at wileyonlinelibrary.com]

where Coeff = A or B, and t' is determined via an empirical model[22] at the compositions that are 50% doped on the A site for divalent dopants and 25% doped on the A site for monovalent dopants (ie, $A^{3+}_{0.5}A^{2+}_{0.5}B^{3+}_{0.5}B^{4+}_{0.5}O_3$ or $A^{3+}_{0.75}A^{1+}_{0.25}B^{3+}_{0.5}B^{4+}_{0.5}O_3$). For instance, the compound $La_{0.8}Sr_{0.2}MnO_3$ has an x value of 0.2, but Equation 8 would be applied to the $La_{0.5}Sr_{0.5}MnO_3$ composition to determine the values of A and B. Then, Equation 7 can be applied to the actual composition, $La_{0.8}Sr_{0.2}MnO_3$, to predict its c/a value. Table 4 lists the goodness of fits and the coefficients of Equation 8.

It is also apparent from Figure 2 that A and B are not independent parameters; instead, it appears that they are highly correlated and are, in fact, displaced mirror images of each other. Figure 3 shows the correlation between A and B, which is linear. It can be represented by Equation 9:

$$B = -1.975479A + 2.411050 \quad \left(R^2 = 1\right). \tag{9}$$

Equation 9 can be substituted into Equation 7; thus, simplifying the model even further as shown in Equation 10:

$$\frac{c}{a} = A\left(\frac{a_{pc}}{r_{BX}} - 1.975479\right) + 2.411050. \tag{10}$$

Now, Equation 10 allows for the prediction of the perovskite trigonality, c/a, using only a single coefficient, A. This coefficient can now be easily calculated using Equation 8 and the coefficients of Table 4 as:

$$A = (-0.279599t'^5 + 1.428203t'^4 - 2.917000t'^3 + 2.977727t'^2 - 1.519272t' + 0.309941\times10^8). \tag{11}$$

Although the $LiNbO_3$ structure is not actually perovskite, the Nb^{5+} is in sixfold coordination and NbO_6 octahedra are corner-shared, so some of the important structural aspects of perovskite are present. Despite the fact that Li^+ is also in octahedral coordination (rather than cuboctahedral) and that LiO_6 octahedra share faces with NbO_6 octahedra, a similar analysis can be undertaken on such compounds. Interestingly, these perovskite-related compounds with $R3c$ symmetry tend to exhibit c/a values greater than $\sqrt{6}$, which is beyond the range of Equations 10 and 11. For this reason, another

TABLE 7 Application of the model to 15 rare-earth-doped aluminates

ICSD #	Compound	$a_{pc(Exptl.)}$ (Å)	$r_{B\text{-}X(Exptl.)}$ (Å)	t' (Equation 3)	c/a Exptl	c/a Calc	|Error%|
191 409	$LaAlO_3$	3.7877	1.896	1.0176	2.4487	2.4348	0.5705
90 558	$PrAlO_3$	3.7630	1.895	0.9994	2.4329	2.4291	0.1575
187 390	$Nd_{0.9}Gd_{0.1}AlO_3$	3.7475	1.89	0.9880	2.4261	2.4209	0.2163
187 391	$Nd_{0.85}Gd_{0.15}AlO_3$	3.7469	1.893	0.9876	2.4252	2.4169	0.3443
258 031	$Nd_{0.95}Tb_{0.05}AlO_3$	3.7490	1.893	0.9891	2.4266	2.4183	0.3406
258 032	$Nd_{0.9}Tb_{0.1}AlO_3$	3.7481	1.89	0.9885	2.4258	2.4214	0.1809
258 041	$Nd_{0.97}Dy_{0.03}AlO_3$	3.7486	1.889	0.9888	2.4269	2.4231	0.1556
258 042	$Nd_{0.95}Dy_{0.05}AlO_3$	3.7462	1.893	0.9871	2.4266	2.4165	0.4159
258 044	$Nd_{0.9}Dy_{0.1}AlO_3$	3.7465	1.894	0.9873	2.4261	2.4155	0.4357
167 500	$Pr_{0.76}La_{0.24}AlO_3$	3.7689	1.895	1.0038	2.4352	2.4349	0.0106
—	$NdAlO_3$[26]	3.7516	1.89	0.9910	2.4279	2.4249	0.1235
—	$Nd_{0.8}Sm_{0.2}AlO_3$[26]	3.7500	1.89	0.9899	2.4268	2.4233	0.1475
—	$Pr_{0.88}Sm_{0.12}AlO_3$[27]	3.7586	1.90	0.9962	2.4311	2.4151	0.6586
—	$Pr_{0.76}Sm_{0.24}AlO_3$[27]	3.7562	1.90	0.9944	2.4300	2.4132	0.6954
—	$Pr_{0.7}Sm_{0.3}AlO_3$[27]	3.7538	1.90	0.9927	2.4297	2.4115	0.7493

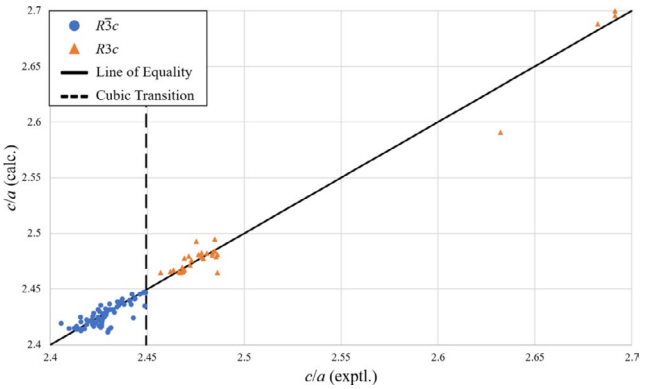

FIGURE 6 Predicted *c*/*a* values of trigonally distorted perovskites and $LiNbO_3$ type structures using Equations 10-12 [Color figure can be viewed at wileyonlinelibrary.com]

general model was developed to describe the trigonality of these compounds.

Figure 4 shows that the trigonality for all 31 *R*3*c* compounds can be represented by the same general quadratic function (Equation 12) in terms of the ratio of the experimental pseudocubic lattice constant, $a_{pc(Exptl.)}$, to the experimental B-X bond length, $r_{B\text{-}X(Exptl.)}$.

$$\frac{c}{a} = 22.211002\left(\frac{a_{pc}}{r_{BX}}\right)^2 - 87.942060\left(\frac{a_{pc}}{r_{BX}}\right) + 89.514066 \quad \left(R^2 = 0.9783\right). \tag{12}$$

Table 5 shows the experimental data and the predicted trigonality for all 31 *R*3*c* trigonal compounds using Equation 12. Overall, this model is very accurate. The average error is 0.2380%. Only the $LiReO_3$ composition produces a rather large error of 1.5779%.

Table 6 shows the experimental and predicted lattice constants for all 31 *R*3*c* trigonal compounds. The average error for *a* and *c* are 0.0795% and 0.1587%, respectively. Again, the $LiReO_3$ composition produces the most error (0.5316% for *a* and 1.0547% for *c*). One of the reasons $LiReO_3$ produces the largest error may be due to the fact that the ReO_3 structure is actually a perovskite[25] with a completely vacant A site; thus, a hybrid $Li_{1-x}(Re^{6+}_{x}Re^{5+}_{1-x})O_3$ may exist here in which a mixture of both Re^{5+} and Re^{6+} share the B site and Li^+ ions only partially occupy the A site, either of which effects would significantly affect the *c*/*a* ratio and cause large errors in both the prediction of trigonality and lattice constants.

Equation 13 describes the mathematical relationship between *c*/*a* and the pseudocubic lattice constant, a_{pc}:

$$\frac{c}{a} = 4\sqrt{3}\left(\frac{a_{pc}}{a}\right)^3. \tag{13}$$

From this expression, it can be shown that the trigonal-to-cubic transition occurs at $c/a = \sqrt{6}$, where the structure is considered trigonal if $c/a \neq \sqrt{6}$. It should also be noted that using Equations 10-13 to predict lattice constants for the cubic perovskite $SrTiO_3$ ($t' = 1$, $a_{pc}/r_{BX} = 2$), the model predicts $c/a = 2.4561$, which is very near the experimental value of 2.4495 (0.270% error). Thus, the model can accurately predict the composition at which a trigonal-to-cubic transition occurs. The trigonal lattice constants can now be derived using Equations 10-13. Figure 5 and Tables 2 and 6 show the predicted trigonal lattice constants using this model and demonstrate that the model is an effective predictive

TABLE 8 Experimental and calculated trigonal lattice constants from Equation 10, 11, and 13 for the 15 rare-earth-doped aluminates in Table 7

ICSD #	Compound	$a_{(Exptl.)}$ (Å)	$a_{(Calc.)}$ (Å)	|Error%|	$c_{(Exptl.)}$ (Å)	$c_{(Calc.)}$ (Å)	|Error%|
191 409	$LaAlO_3$	5.3572	5.3674	0.1909	13.1183	13.0684	0.3807
90 558	$PrAlO_3$	5.3337	5.3365	0.0526	12.9766	12.9630	0.1050
187 390	$Nd_{0.9}Gd_{0.1}AlO_3$	5.3167	5.3205	0.0722	12.8991	12.8805	0.1443
187 391	$Nd_{0.85}Gd_{0.15}AlO_3$	5.3165	5.3226	0.1150	12.8936	12.8640	0.2297
258 031	$Nd_{0.95}Tb_{0.05}AlO_3$	5.3185	5.3245	0.1138	12.9056	12.8763	0.2272
258 032	$Nd_{0.9}Tb_{0.1}AlO_3$	5.3178	5.3210	0.0604	12.9000	12.8844	0.1207
258 041	$Nd_{0.97}Dy_{0.03}AlO_3$	5.3176	5.3204	0.0519	12.9055	12.8921	0.1037
258 042	$Nd_{0.95}Dy_{0.05}AlO_3$	5.3146	5.3220	0.1390	12.8963	12.8605	0.2775
258 044	$Nd_{0.9}Dy_{0.1}AlO_3$	5.3154	5.3231	0.1457	12.8955	12.8580	0.2907
167 500	$Pr_{0.76}La_{0.24}AlO_3$	5.3404	5.3406	0.0035	13.0049	13.0040	0.0071
—	$NdAlO_3$[26]	5.3212	5.3233	0.0412	12.9195	12.9088	0.0823
—	$Nd_{0.8}Sm_{0.2}AlO_3$[26]	5.3197	5.3223	0.0492	12.9102	12.8975	0.0983
—	$Pr_{0.88}Sm_{0.12}AlO_3$[27]	5.3288	5.3405	0.2205	12.9550	12.8981	0.4395
—	$Pr_{0.76}Sm_{0.24}AlO_3$[27]	5.3262	5.3386	0.2329	12.9429	12.8828	0.4641
—	$Pr_{0.7}Sm_{0.3}AlO_3$[27]	5.3231	5.3365	0.2510	12.9334	12.8687	0.5002

tool at least within the ranges $5.3594 \leq a \leq 5.5776$ and $12.9828 \leq c \leq 13.5470$ provided that $2.406 \leq c/a \leq 2.4495$ for $R\bar{3}c$ symmetry; and $5.0918 \leq a \leq 5.8461$ and $13.4030 \leq c \leq 14.4182$ provided that $2.4495 \leq c/a \leq 2.6913$ for $R3c$ symmetry.

Tables 7 and 8 show an application of this modeling technique. In particular, the model has been applied to 15 trigonally distorted aluminate perovskites as found in literature. Table 7 shows that the model is very accurate when used to calculate the c/a ratios for these compounds.

Figure 6 shows the predicted trigonality using the general models. The accuracy of the models appears to be very good for all 72 trigonally distorted perovskites and 31 $LiNbO_3$ type structures analyzed in this work. It shows that the models can be applied even to compositions that are severely distorted on either side of the cubic transition. There appears to be an outlier at $c/a \sim 2.42$, which corresponds to $La_{0.67}Pb_{0.33}MnO_3$.[28] The underestimation of the trigonality in this case may be due to excessive lead volatilization during sintering, especially as this sample was sintered five times in an open environment, likely causing the formation of oxygen vacancies which would be virtually undetectable via XRD. The reasons for the outlier at $c/a \sim 2.63$, which corresponds to $LiReO_3$; have already been addressed.

It is also useful to relate trigonality to polarization, which is the intrinsic component of the relative permittivity—the

TABLE 9 Room-temperature polarizations of 31 trigonal compositions in space group $R3c$

ICSD	Data Type	Compound	$c/a_{(exptl.)}$	Polarization ($\mu C/cm^2$)$_{(exptl.)}$	Polarization ($\mu C/cm^2$)$_{(calc.)}$	|Error%|
250 775	Neutron	$LiNbO_3$	2.6869	66.2863	61.5224	7.19
35 012	Neutron	$LiReO^3$	2.6323	20.1141	23.0340	14.52
98 123	neutron	$(Li_{0.937}Zn_{0.063})(Nb_{0.0979}Zn_{0.021})O_3$	2.6913	62.1352	66.6244	7.23
98 125	Neutron	$(Li_{0.94}Zn_{0.06})(Nb_{0.98}Zn_{0.02})O_3$	2.6913	62.9878	66.6244	5.77
250 774	Neutron	$Li_{0.96}Na_{0.04}NbO_3$	2.6824	62.3474	56.7818	8.93
46 024	Neutron	$PbZr_{0.9}Ti_{0.1}O_3$	2.4681	41.9707	41.6220	0.83
193 811	neutron	$Bi_{0.5}Na_{0.5}TiO_3$	2.4569	16.1952	16.9870	4.89
280 368	Neutron	$PbHf_{0.8}Ti_{0.2}O_3$	2.4635	34.5167	31.5550	8.58
86 131	Neutron	$PbZr_{0.871}Ti_{0.129}O_3$	2.4663	37.7467	37.7171	0.08
86 132	Neutron	$PbZr_{0.838}Ti_{0.162}O_3$	2.4670	42.4012	39.1793	7.60
86 133	Neutron	$PbZr_{0.796}Ti_{0.204}O_3$	2.4678	42.6230	40.9237	3.99
86 134	Neutron	$PbZr_{0.745}Ti_{0.255}O_3$	2.4684	41.0485	42.4230	3.35
86 135	Neutron	$PbZr_{0.7}Ti_{0.3}O_3$	2.4691	38.4811	43.7901	13.80
237 367	Neutron	$BiFeO_3$	2.4862	72.0989	71.2317	1.20
237 369	Neutron	$BiCo_{0.2}Fe_{0.8}O_3$	2.4788	67.9923	65.3965	3.82
261 637	Neutron	$Bi_{0.95}Tb_{0.05}FeO_3$	2.4837	69.8951	69.7663	0.18
261 638	Neutron	$Bi_{0.9}Tb_{0.1}FeO_3$	2.4837	67.6325	69.7663	3.16
261 639	Neutron	$Bi_{0.85}Tb_{0.15}FeO_3$	2.4807	67.5440	67.2695	0.41
182 003	Neutron	$Bi_{0.88}Sm_{0.12}FeO_3$	2.4781	57.2301	64.6766	13.01
194 413	Neutron	$Bi_{0.9}La_{0.1}FeO_3$	2.4754	55.9634	61.6084	10.09
181 565	Neutron	$Bi_{0.815}La_{0.185}FeO_3$	2.4693	45.1479	53.9537	19.50
193 689	neutron	$BiFe_{0.98}Co_{0.02}O_3$	2.4855	70.2511	70.9030	0.93
82 615	Neutron	$Bi_{0.93}La_{0.07}FeO_3$	2.4765	65.8305	62.9056	4.44
51 662	Neutron	$BiMn_{0.2}Fe_{0.8}O_3$	2.4780	68.4157	64.5531	5.65
51 663	Neutron	$BiMn_{0.1}Fe_{0.9}O_3$	2.4834	70.4312	69.5379	1.27
192 514	Neutron	$Bi_{0.95}Dy_{0.05}FeO_3$	2.4848	69.6892	70.5094	1.18
165 908	Neutron	$Bi_{0.85}La_{0.15}FeO_3$	2.4848	71.8443	70.5094	1.86
187 231	Neutron	$Bi_{0.87}La_{0.13}FeO_3$	2.4728	61.0800	58.5831	4.09
188 046	Neutron	$BiFe_{0.9}Ti_{0.1}O_3$	2.4721	59.0363	57.6591	2.33
252 624	Neutron	$Bi_{0.9}Pb_{0.1}FeO_3$	2.4619	42.9346	41.7655	2.73
163 686	Neutron	$Bi_{0.9}Ca_{0.1}FeO_3$	2.4714	64.4325	56.7831	11.87

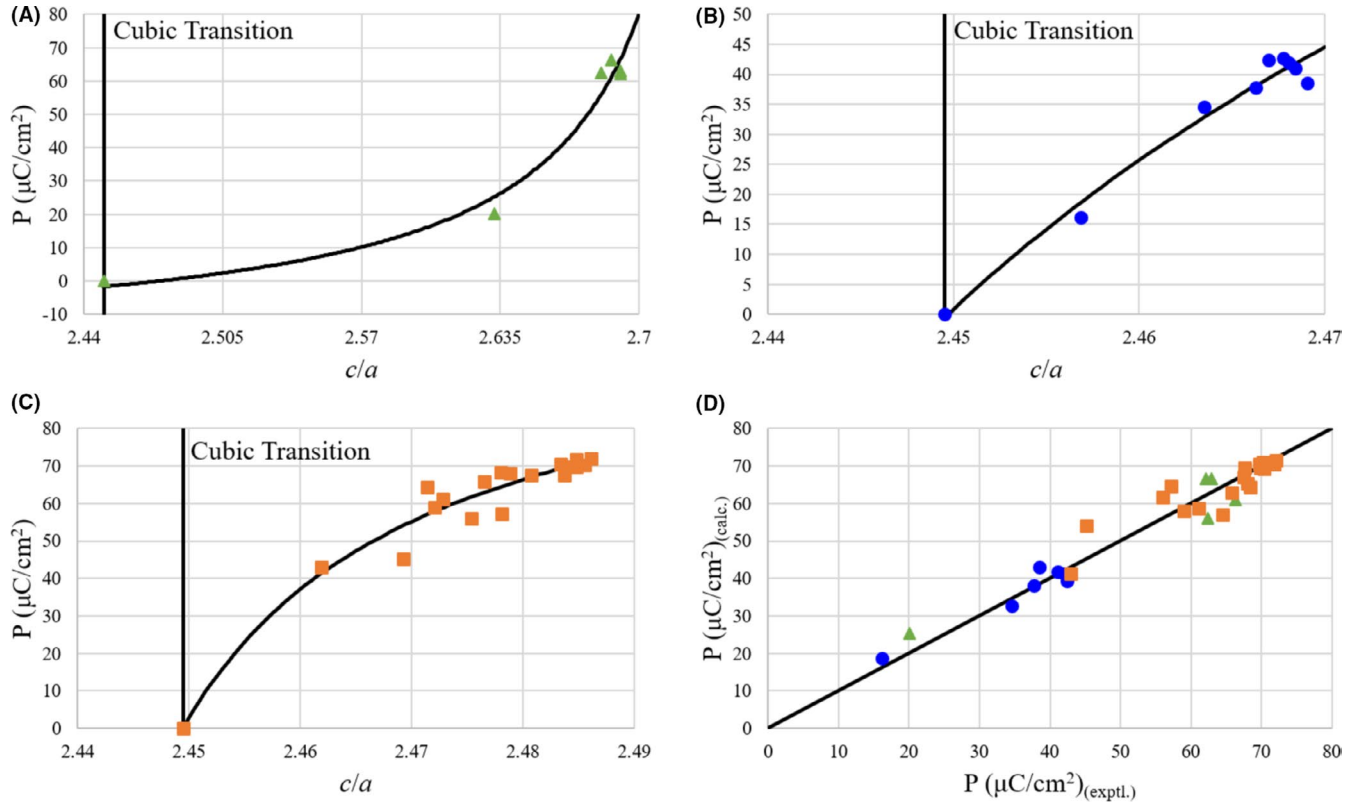

FIGURE 7 Polarization of the 31 compositions in space group *R*3*c* of the form (A) $A^{1+}B^{5+}O_3$, (B) $A^{2+}B^{4+}O_3$, and (C) $A^{3+}B^{3+}O_3$ as a function of *c*/*a*. (D) Calculated vs experimental polarization values for all 31 *R*3*c* compositions. All experimental data are from neutron diffraction [Color figure can be viewed at wileyonlinelibrary.com]

key to unlocking the ferroelectric, piezoelectric, and pyroelectric properties of a material. The dipole moment of a material arises from the separation of the two oppositely charged sublattices. There is obviously no net dipole moment for perovskites in the centrosymmetric space group $R\bar{3}c$, in which the charge centers of the two sublattices coincide. On the other hand, space group *R*3*c* is non-centrosymmetric; thus, perovskites and other compounds with *R*3*c* symmetry can have non-zero dipole moments. Table 9 shows the derived polarizations for 31 *R*3*c* trigonal compounds which are the direct result of their trigonal distortion. Figure 7 shows that there are three distinct trends in polarization which coincide with $A^{1+}B^{5+}O_3$, $A^{2+}B^{4+}O_3$, and $A^{3+}B^{3+}O_3$ structures. This distinction between compounds with larger charge differences between the A and B cations and ones with equally charged A and B cations makes sense because the charge centers for the cation sublattices will be different depending upon the ionic charges of the A- and B-site cations. The trends in each of these cases are described by Equations 14-16.

Figure 7 shows that all three polarization trends can be described by the same general equation:

$$P\left[\frac{\mu C}{\mathrm{cm}^2}\right] = G\tan\left(H\left(\frac{c}{a}\right) - \sqrt{6}\right) + K, \qquad (14)$$

TABLE 10 Coefficients of Equation 14

Series	*G*	*H*	*K*	R^2
$A^{+}B^{5+}O_3$	−4.515086	−0.821300	−19.295296	0.9675
$A^{2+}B^{4+}O_3$	18.720362	1.683688	178.895349	0.9749
$A^{3+}B^{3+}O_3$	18.581938	8.123501	108.231639	0.9469

where $H(c/a) - \sqrt{6}$ is in radians. It should be noted that the $P = 0$ data point at $c/a = \sqrt{6}$ was assumed in all three cases because the polarization will be zero when the structure transitions from trigonal to the centrosymmetric cubic space group $Pm\bar{3}m$. Table 10 lists the coefficients for each series.

Figure 8 shows that all three coefficients of Equation 14 can be represented by the same expression as a function of the charge difference between the A- and B-site species, Δq:

$$\mathrm{Coeff} = M\sin(0.8\Delta q) + Q\cos(0.45\Delta q), \qquad (15)$$

where Coeff = *G*, *H*, or *K*. Table 11 shows the coefficients of Equation 15.

Although Figure 8 clearly shows that *G*, *H*, and *K* are not correlated, the coefficients of those fits (*M* and *Q*) are, in fact, highly correlated, as shown in Figure 9, and can be represented by Equation 16.

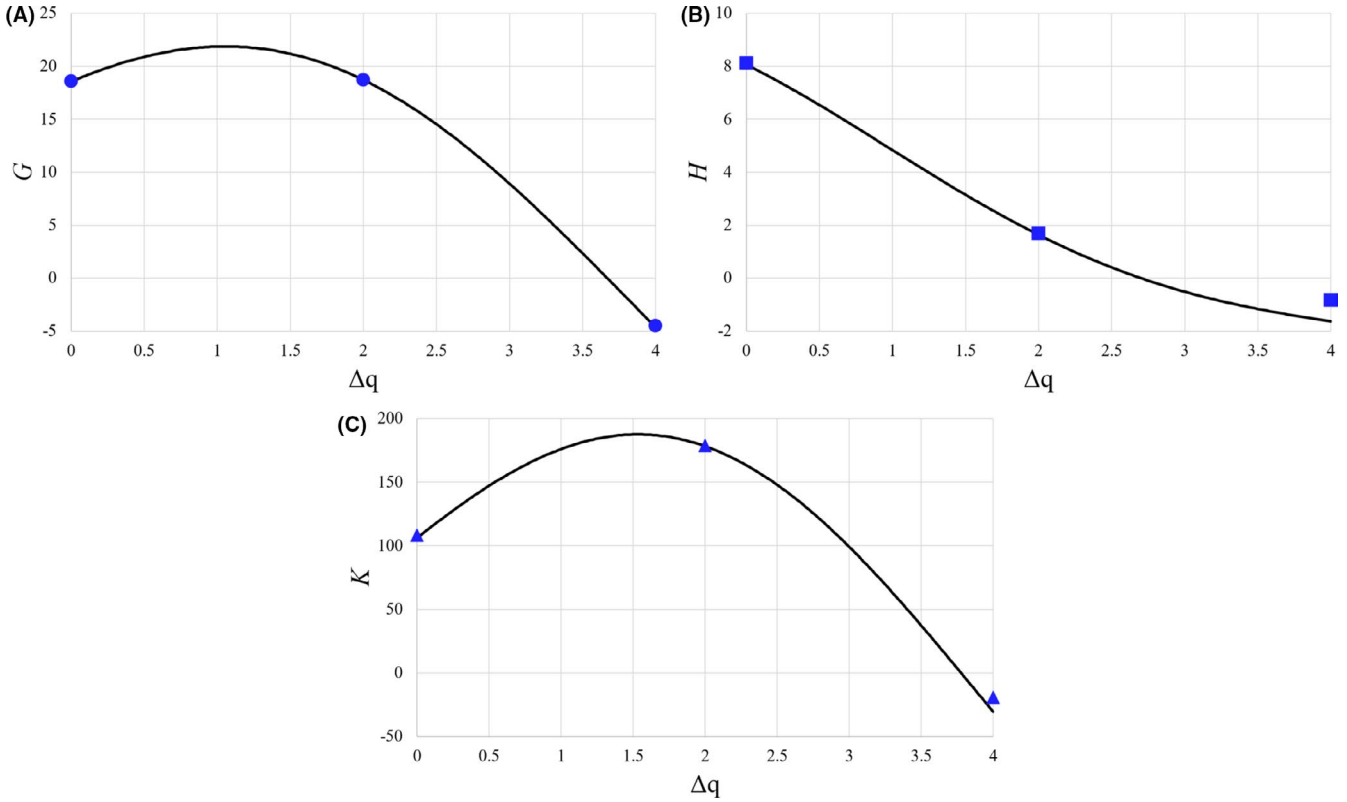

FIGURE 8 Coefficients of Equation 14 as functions of the charge difference between the A- and B-site cations, Δq [Color figure can be viewed at wileyonlinelibrary.com]

Figure 9 clearly shows that M and Q can be represented in terms of one another as illustrated by Equation 16:

$$Q = 0.840861M + 11.669807, \tag{16}$$

Thus, Equation 15 can be simplified as follows:

$$\text{Coeff} = M\left(\sin\left(0.8\Delta q\right) + 0.840861\cos\left(0.45\Delta q\right)\right) + 11.669807\cos\left(0.45\Delta q\right), \tag{17}$$

Although $Bi_{0.9}Pb_{0.1}FeO_3$ and $Bi_{0.9}Ca_{0.1}FeO_3$ are not exactly $A^{3+}B^{3+}O_3$ type compounds, their ionic charges are very close; hence, they fit the trend very well. It should also be noted that all the data used for deriving the polarization trends are from neutron diffraction experiments because, unlike XRD, neutron diffraction is sensitive to oxygen positions. Thus, structural data derived from neutron diffraction experiments will provide the most accurate positions for the oxygen sublattice, which will allow for the polarization to be more accurately calculated from that structural data.

4 | CONCLUSIONS

Using data mined from literature for several specific systems, general models were derived for the trigonality of perovskites in $R\bar{3}c$ and $LiNbO_3$ type compounds in $R3c$ as a function of the ratio of pseudocubic lattice constant, a_{pc}, to B-X bond length, r_{BX}. A major implication of these models is that they allow for the accurate prediction of trigonal lattice parameters in trigonally distorted perovskites and $LiNbO_3$ type compounds. In addition, these models successfully predicted the trigonal-to-cubic phase transition at room temperature. It may even be possible to extend these models, in conjunction with other empirical models, to predict temperature-dependent trigonal phase transitions in perovskites (eg, T_C). Moreover, a general model has been developed for predicting the polarization in trigonal $LiNbO_3$ type compounds of the forms $A^{1+}B^{5+}O_3$, $A^{2+}B^{4+}O_3$, and $A^{3+}B^{3+}O_3$ in $R3c$. This model has major implications in the electroceramics industry because it allows for the accurate prediction of intrinsic polarization using only the c/a ratio, which itself can be accurately predicted using the models presented here.

TABLE 11 Coefficients of Equation 15

Coefficient	M	Q	R^2
G	7.179977	18.558904	1.0000
H	−3.374372	8.058375	0.9842
K	112.350064	106.062864	0.9933

ACKNOWLEDGMENTS

This work has been supported by the Micron School of Materials Science and Engineering at Boise State University.

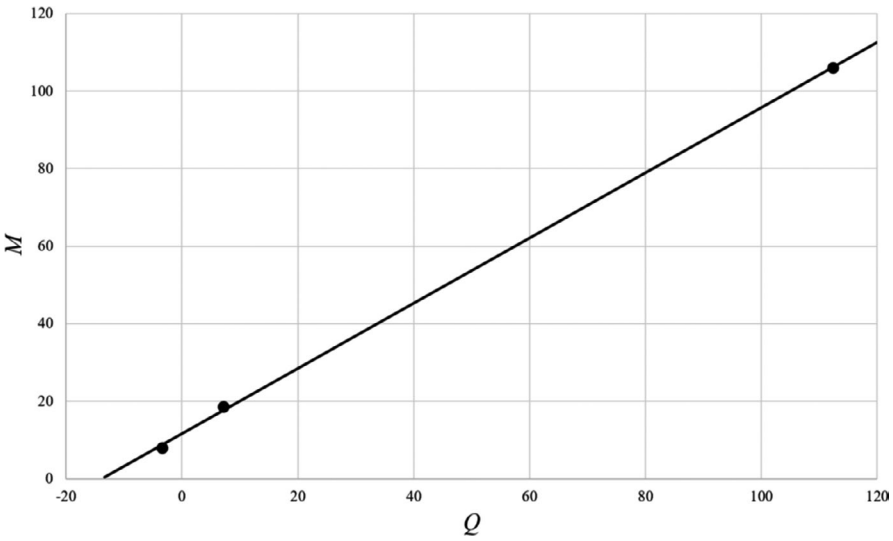

FIGURE 9 Correlation between the coefficients of Equation 15

ORCID

Evan Smith https://orcid.org/0000-0002-1603-0517
Rick Ubic https://orcid.org/0000-0003-4813-3462

REFERENCES

1. Zenmi S, Ja D, Cherif K, Je D, Oummezzine M, Ghedira M, et al. The effect of a cation radii on structural, magnetic and electrical properties of doped manganites $La_{0.6-x}Pr_xSr_{0.4}MnO_3$. J Solid State Chem. 2004;177:2387–93.
2. Anwar M, Kumar S, Ahmed F, Arshi N, Koo B. Structural, magnetic and magnetocaloric properties of $La_{0.65}Sr_{0.35}V_{0.1}Mn_{0.9}O_3$ perovksite. Mater Res Bull. 2012;47:2977–9.
3. Ifrah S, Kaddouri A, Gelin P, Leonard D. Hydrothermal synthesis of $La_{1-x}Ag_xMnO_3$ (x = 0,0.2) perovskites used in methane combustion. C R Chimie. 2007;10:1216–26.
4. Sosnowska I, Azuma M, Przenioslo R, Wardecki D, Chen W, Oka K, et al. Crystal and magnetic structure in Co-substituted $BiFeO_3$. Inorg Chem. 2013;52:13269–77.
5. Glazer AM. The classification of tilted octahedra in perovskites. Acta Crystallogr Sec B. 1972;28:3384–92.
6. Tilley JD. Perovskites: structure-property relationships. West Sussex, UK: John Wiley & Sons, Ltd; 2016.
7. Grocholski B, Shim S, Sturhahn W, Zhao J, Xiao Y, Chow P. Spin and valence states of iron in $(Mg_{0.8}Fe_{0.2})SiO_3$ perovskite. Geophys Res Lett. 2009;36(24):L24303.
8. Sidey V. A simplified empirical model for predicting the lattice parameters of the cubic/pseudocubic perovskites. J Solid State Chem. 2019;279:120951.
9. Jiang L, Guo J, Liu H, Zhu M, Zhou X, Wu P, et al. Prediction of lattice constant in cubic perovskites. J Phys Chem Solids. 2006;67(7):1531–6.
10. Ubic R. Revised method for the prediction of lattice constants in cubic and pseudocubic perovskites. J Am Ceram Soc. 2007;90(10):3326–30.
11. Ubic R, Subodh G. The prediction of lattice constants in orthorhombic perovskites. J Alloys Compd. 2009;488(1):374–9.
12. Kumar A, Verma A. Lattice constant of orthorhombic perovskite solids. J Alloys Compd. 2009;480(2):650–7.
13. Tolman K, Ubic R. An empirical model for perovskite tetragonality. J Alloys Compd. 2017;690:825–35.
14. Lufaso M, Woodward P. Prediction of the crystal structures of perovskites using the software program SPuDS. Acta Crystallogr Sect B Struct Sci. 2001;57:725–38.
15. Salinas-Sanchez A, Garcia-Munoz J, Rodriguez-Carvajal J, Saez-Puche R, Martinez J. Structural characterization of R2BaCuO5 (R = Y, Lu, Yb, Tm, Er, Ho, Dy, Gd, Eu and Sm) oxides by X-ray and neutron diffraction. J Solid State Chem. 1992;100(2):201–11.
16. Goldschmidt V. The laws of crystal chemistry. Naturwisenschaften. 1926;14:477–85.
17. Shannon R. Revised effective ionic-radii and systematic studies of interatomic distances in halides and chalcogenides. Acta Crystallogr Sec A. 1976;32:751–67.
18. Bartel C, Sutton C, Goldsmith B, Ouyang R, Musgrave C, Ghiringhelli L, et al. New tolerance factor to predict the stability of perovskite oxides and halides. Sci Adv. 2019;5(2):eaav0693.
19. Ubic R, Subodh G, Sebastian M, Gout D, Proffen T. Effective size of vacancies in the $Sr_{1-3x/2}Ce_xTiO_3$ superstructure. Ceram Trans. 2009;204:177–85.
20. Ubic R, Tolman K, Chan K, Lundy N, Letourneau S, Kriven W. Effective size of vanancies in aliovalently doped $SrTiO_3$ perovskites. J Alloys Compd. 2013;575:239–45.
21. Tolman K, Ubic R, Papac M. Structural effect of aliovalent doping in lead perovskites. J Solid State Chem. 2015;225:359–67.
22. Ubic R, Tolman K, Talley K, et al. Lattice-constant prediction and effect of vacancies in aliovalently doped perovskites. J Alloys Compd. 2015;644:982–95.
23. Smith E, Ubic R. Empirical models for layered A-site ordering in perovskite titanates. J Am Ceram Soc. 2019;102:3019–31.
24. Smith E, Adams C, Ubic R. Correlative models for perovskites with rock salt B-site ordering. J Am Ceram Soc. 2020;103:577–88.
25. Jorgensen JE, Jorgensen JD, Batlogg B, Remeika JP, Axe JD. Order parameter and critical exponent for the pressure-induced phase transitions in ReO_3. Phys Rev B. 1986;33:4793–8.

26. Yoshikawa A, Saitow A, Horiuchi H, Shishido T, Fukuda T. Orthorhombic to trigonal phase transition of perovskite-type $(Nd_xSm_{1-x})AlO_3$. J Alloys Compd. 1998;266:104–10.
27. Basyuk T, Vasylechko L, Fadeev S, Berezovets V, Trots D, Niewa R. Phase and structural behaviour of the $PrAlO_3$-$SmAlO_3$ system. Acta Phys Pol, A. 2010;117:98–103.
28. Dhahri N, Dhahri A, Cherif K, Dhahri J, Taibi K, Dhahri E. Structural, magnetic and electrical properties of $La_{0.67}Pb_{0.33}Mn_{1-x}Co_xO_3$ ($0 \leq x \leq 0.3$). J Alloys Compd. 2010;496:69–74.

How to cite this article: Smith E, Wander O, Ubic R. Empirical models of trigonal distortions and polarization in perovskites. *J Am Ceram Soc*. 2020;103:7172–7187. https://doi.org/10.1111/jace.17400